Luo *et al. Stem Cell Research & Therapy* (2025) 16:350
https://doi.org/10.1186/s13287-025-04491-3

Stem Cell Research & Therapy

RESEARCH Open Access

Single-cell transcriptome atlas reveals mitophagy dynamics in acute chemical injury model and the role of MSCs transplantation

Sang Luo[1*], Fang Wu[2] and Xiaojun Yang[3*]

Abstract

Background and purpose Mitochondrial autophagy, also referred to as mitophagy, clears damaged mitochondria and has dual functions in disease development and liver homeostasis in response to liver pathologies. Mesenchymal stem/stromal cells (MSCs) are most commonly used to treat liver failure because they are easy to obtain and present no ethical problems. However, the molecular mechanisms by which MSCs promote liver failure progression are not fully understood. This study explored the distinct mitophagy states in hepatocytes and macrophages during MSCs therapy.

Experimental approach To investigate tissue-specific mitophagy in acute liver failure (ALF), we generated a single-cell transcriptome (scRNA-seq) atlas of liver tissue from healthy mice, ALF mice and human umbilical cord mesenchymal stem/stromal cell (hUC-MSC)-transplanted mice.

Key results The data revealed the complex cellular landscape of liver tissue during ALF progression, revealing alterations in metabolic fluxes and mitophagy activation. Through the intersection of single-cell sequencing data with mitophagy-related genes (MRGs), a total of 24 differentially expressed MRGs were identified. Gene Ontology (GO) analysis further revealed that the ubiquitinating enzyme Arih1 was significantly upregulated after MSC transplantation, whereas the mitophagy genes Bnip3L/NIX and Beciln1 were significantly downregulated in mononuclear phagocytes(MPs).

Conclusions and implications Our research demonstrated that during the development of ALF, mitophagy within hepatocytes is suppressed, whereas in MPs, mitophagy is excessively activated. MSCs are capable of alleviating disease progression by modulating the distinct mitophagy states of cells, providing an important resource for investigating mitophagy regulation in hepatic homeostasis and disease development.

Keywords Mitophagy, Liver failure, Mesenchymal stem/stromal cells

*Correspondence:
Sang Luo
175919898@qq.com
Xiaojun Yang
yxjicu@163.com
[1]Department of Beijing National Biochip Research Center Sub-Center in Ningxia, Institute of Medical Sciences, General Hospital of Ningxia Medical University, No. 804 Shengli South Street, Xingqing District, Yinchuan 750004, Ningxia, China
[2]Ningxia Regional Key Laboratory of Integrated Traditional Chinese and Western Medicine for Prevention and Treatment of Regional High Incidence Disease, Ningxia Medical University, Yinchuan 750004, Ningxia, China
[3]General Hospital of Ningxia Medical University, No. 804 Shengli South Street, Xingqing District, Yinchuan 750004, Ningxia, China

Introduction

The liver, the key metabolic centre in humans, contributes to multiple physiological processes, e.g., the biotransformation of nutrients and xenobiotics and detoxification [1]. Liver disease, e.g., acute liver failure (ALF), has a mortality rate of approximately 30% [2] and is considered a growing health threat globally, although its aetiological mechanisms differ substantially in various regions [3]. In underdeveloped nations, acute viral hepatitis is the major factor causing ALF [4]; in Asian and Mediterranean countries specifically, ALF is caused mostly by hepatitis B virus (HBV) infection [5, 6]. However, with the popularization of HBV vaccination in China and the gradual decrease in HBV carriage in the human population, the incidence of ALF caused by drug-related injuries is gradually increasing [7], which is also the main form of ALF in Western countries. ALF is a serious condition in which swift hepatocyte necrosis may result in rapid death, with high medical costs. Therefore, clarifying the pathogenetic mechanisms of ALF and identifying molecular targets for its prevention are urgently needed.

Under stress, hepatocytes undergo metabolic reprogramming to compensate for these new conditions. Mitochondria constitute the main organelles that produce ATP in cells via the tricarboxylic acid cycle and oxidative phosphorylation [8]. In response to external stressors, impaired mitochondria synthesize high amounts of reactive oxygen species, causing cell damage [9–12]. Mitophagy is a major physiological process in mitochondrial dysfunction, allowing the self-degradation of dysfunctional or excess mitochondria to maintain hepatic function and to protect against tissue damage [13].

However, several studies have shown that mitophagy is unable to reach sufficiently high levels to repair the damaged tissue under injury conditions [14]. In contrast, other reports have suggested that mitophagy may be overactivated during disease development; specifically, there is an upper limit of mitophagy activation beyond which tissue/organ degeneration may result [15, 16]. The extent of mitophagy activation during ALF development remains unknown. A comprehensive understanding of the role of mitophagy in ALF may help researchers to develop novel therapeutic and intervention strategies. In this study, we employed single-cell sequencing (scRNA-seq) to identify differentially expressed mitophagy-related genes (DE-MRGs) between ALF and hUC-MSC-implanted liver tissues at single-cell resolution, quantified the expression of DE-MRGs in various cell clusters, and performed trajectory analyses. Additionally, our findings were confirmed by qRT-PCR and transmission electron microscopy (TEM). Our study was aimed at clarifying the novel mechanism of the mitophagy pathway in the ALF process.

Results

Establishment of an ALF mouse model

For single-cell sequencing, selecting a suitable mouse model that closely mimics the pathophysiological features of ALF is crucial. Therefore, we investigated the impacts of administering different doses of carbon tetrachloride (CCl_4) on the livers of mice. Five experimental groups were set up, with CCl_4 doses of 2.5 mL/kg, 5 mL/kg, 6 mL/kg, 7 mL/kg, and 10 mL/kg, along with a control group. Initially, the survival rates of these mice were documented within 7 days. Compared with age-matched, uninjured mice (control group), mice treated with 2.5 mL/kg CCl_4 demonstrated robust self-recovery. In contrast, the survival rates of the 5 mL/kg and 10 mL/kg groups were lower than those of the other groups at 72 h and 12 h, respectively (Fig. 1a); concomitantly, the histological features and function of the livers were altered. Compared with those in the control mice, the serum alanine aminotransferase (ALT), aspartate aminotransferase (AST), and total bile acid (TBA) levels were substantially elevated in the 2.5 mL/kg, 5 mL/kg and 7 mL/kg groups, respectively. Moreover, the amounts of albumin (ALB) and total bilirubin (TBIL) strongly decreased (Fig. 1b-f).

In the above three injection groups (2.5 mL/kg, 5 mL/kg and 7 mL/kg), characteristic focal lesions were detected around the hepatic central vein. These lesions included moderate-to-severe liver oedema, steatosis, necrosis, and infiltration of immune cells. Compared with those in the 5 mL/kg CCl_4 group, the livers in the 2.5 mL/kg CCl_4 group presented more severe liver oedema, steatosis, and necrosis, along with a greater influx of immune cells at the corresponding time points (Fig. 1g, h). Concurrently, the levels of proinflammatory cytokines such as interleukin-6 (IL-6), IL-1β, and tumour necrosis factor-α (TNF-α) were markedly greater in the 2.5 mL/kg, 5 mL/kg and 7 mL/kg groups. However, no marked differences were detected between the 2.5 mL/kg and 5 mL/kg groups (Fig. 1i). Collectively, these findings suggest that following intraperitoneal injection of 5 mL/kg CCl_4 for 24 h, the liver sustains severe damage, closely mimicking the pathophysiological features of clinical ALF.

Single-cell mt-DNA expression profiles of ALF mice and hUC-MSC-transplanted mice

We performed single-cell sequencing analyses of normal mice, mice with CCl_4-induced acute liver failure (ALF), and mice transplanted with human umbilical cord mesenchymal stem/stromal cells (hUC-MSCs). Through analyses of the differential gene expression in the major cell types, we found that, in the ALF mouse model, the expression levels of mitochondrial genes in MPs and T, NK and B cells were significantly greater than those in the mice transplanted with hUC-MSCs (Fig. 2a,

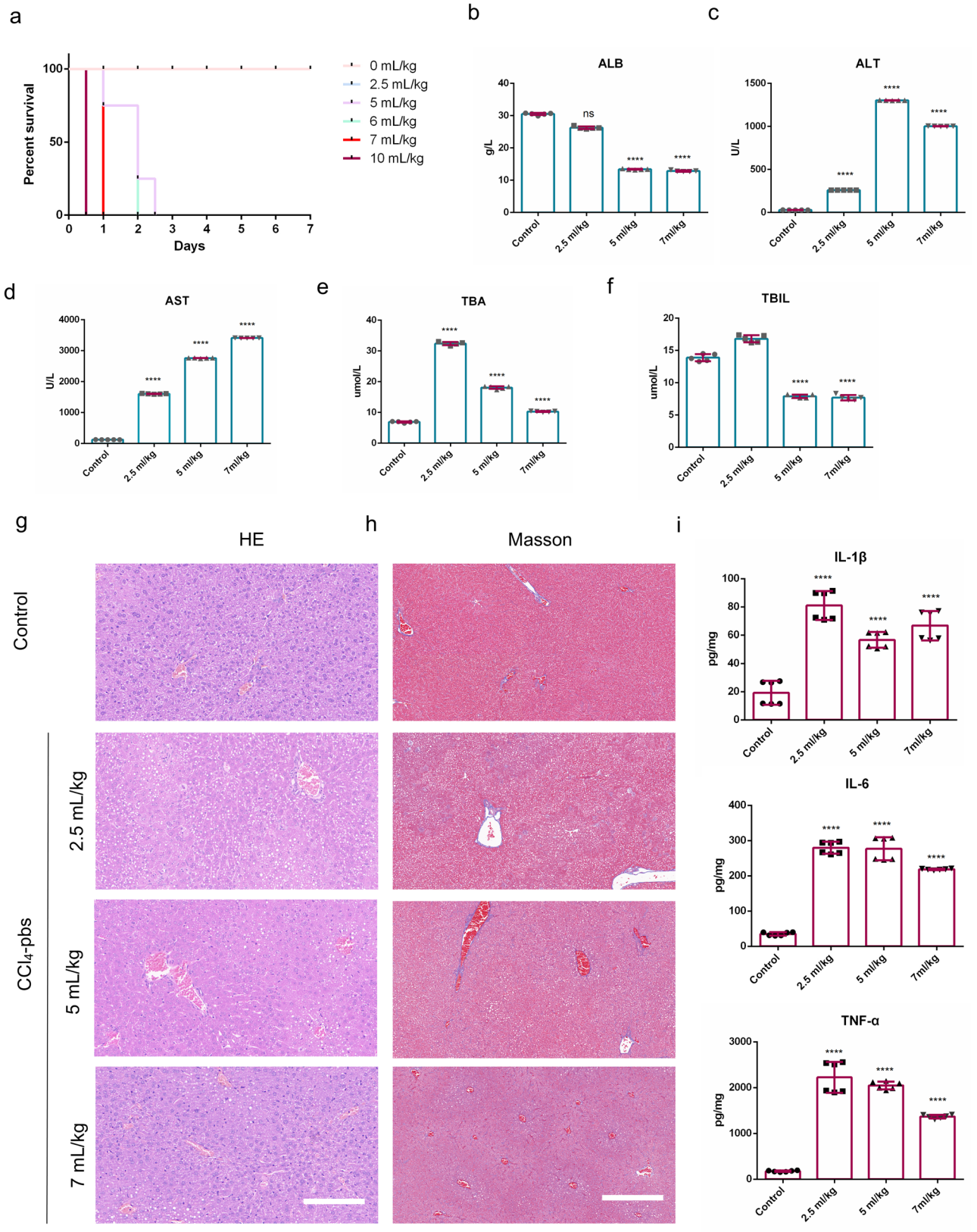

Fig. 1 (See legend on next page.)

(See figure on previous page.)

Fig. 1 Establishment of the ALF Mouse Model **(a)** Survival curves of the various groups of CCl_4-treated mice ($n = 6$/group). **(b-f)**: Serum ALB, ALT, AST, TBA and TBIL levels in the animal models 24 h after treatment with 2.5 ml/kg, 5 ml/kg and 7 ml/kg CCl_4 ($n = 5$/group). Significance is indicated as $^{*}P < 0.05$, $^{**}P < 0.01$, $^{***}P < 0.001$, $^{****}P < 0.0001$, and ns: not significant. **(g)** Haematoxylin and eosin (H&E)-stained images (×40 magnification) of the livers. Scale bar = 50 μm. **(h)** Masson-stained images (× 20 magnification) of the livers. Scale bar = 100 μm. **(i)** ELISA was used to analyse the levels of the proinflammatory factors IL-1β, IL-6 and TNF-α in the livers harvested from each CCl_4-treated group ($n = 6$/group). Significance is indicated as $^{****}P < 0.0001$, and ns: not significant

Figure S1a-h). Furthermore, from the list of differentially expressed genes in all clusters, a total of 13 mitochondrial genes were extracted. Intergroup comparisons revealed that the expression levels of mt-co1, mt-cytb, mt-Nd1, mt-Nd2, and mt-Nd4 were significantly increased in the CCl_4-induced ALF mouse model and that the levels in normal mice and in mice following hUC-MSC transplantation were similar (Fig. 2b), which was consistent with the qRT-PCR results (Fig. 2c). In addition, we observed changes in the mitochondrial structure using transmission electron microscopy (TEM). The microscopy results revealed that in the ALF mouse model, the mitochondria in hepatocytes exhibited sparse cristae, swelling, and a lack of connections, whereas the mitochondrial structure in the liver tissue of the mice after hUC-MSC transplantation was clear, with regularly arranged cristae, indicating that mitochondrial gene expression increased significantly during the development of ALF (Fig. 2d, e).

Metabolic heterogeneity between hepatocytes and MPs in ALF mice

Abnormal metabolism has a pivotal effect on the occurrence and progression of ALF. Consequently, we leveraged gene set variation analysis (GSVA) to compare metabolic pathway activities among the normal, CCl_4-pbs, and CCl_4-hUCMSC groups. In contrast to the amino acid and lipid metabolism pathways, the carbohydrate metabolism pathway was markedly enriched in the ALF mouse model (Fig. 3a). Furthermore, we used single-cell functional enrichment analysis (scFEA) to determine the metabolite abundance levels in diverse cells across different samples with precision. Compared with the normal and CCl_4-hUCMSC groups, methionine was significantly enriched in hepatocytes from the CCl_4-pbs group. In contrast, mononuclear phagocytes (MPs) were notably enriched in threonine and phenylalanine in the normal and CCl_4-hUCMSC groups (Fig. 3b). Nonetheless, no significant disparities in metabolic fluxes were detected among the three groups of mice for either hepatocytes or MPs (Fig. 3c). These findings suggest opposing trends for metabolic abnormalities between hepatocytes and MPs in the ALF mouse model. Specifically, mitochondria-related energy metabolism abnormalities are attenuated in hepatocytes but augmented in MPs.

MSCs alleviate the disrupted state of mitochondrial function in the ALF mouse model

To elucidate the correlation between mitochondrial homeostasis and ALF development, we analyzed the mitochondrial function in different mouse models. We downloaded four datasets related to mitochondrial dysfunction from https://www.gsea-msigdb.org/gsea/msigdb/human/genesets.jsp: GOBP_ATP_SYNTH ESIS _COUPLED_ELECTRON_TRANSPORT (M23564), GOBP_MITOPHAGY (M22148), REACTOME_PINK1_PRKN_MEDIATED_MITOPHAGY (M27419), and REACTOME_RECEPTOR_MEDIATED_MITOPHAGY (M27789). The correlation between mitochondrial function and samples was assessed using Ucell gene set scoring. First, mitochondrial function scores were evaluated for major cell types across the three mouse models. The results revealed that in normal and hUC-MSC-transplanted mice, the lowest scores for major cell types, with the exception of hepatocytes, were obtained for the ATP-coupled electron transfer pathway gene set (Fig. 4a), the mitophagy-related gene (MRG) set (Fig. 4b), the reactome-PINK1-PRKN-mediated mitophagy gene set (Fig. 4c) and the reactome-receptor-mediated mitophagy gene set (Fig. 4d); scores for these gene sets were highest in the ALF (CCl_4-pbs) liver injury model mice; however, the scores of the abovementioned gene sets showed the opposite trend in hepatocytes. Notably, the Ucell scores for the abovementioned four gene sets were markedly elevated in the ALF (CCl_4-pbs) group compared with the normal and CCl_4-hUCMSC transplantation groups (Fig. 4e-h).

We further used the Ucells to score upregulated mitochondria-related pathways in key cell clusters, which are presented in feature plots and box plots. Most of the mitochondria-related pathways had higher scores in hepatocytes than in other cell types. In the normal and CCl_4-hUCMSC transplantation groups, the scores for mitochondria-related pathways in hepatocytes were greater than those in the CCl_4-pbs group. However, the scores for mitochondria-related pathways in the MPs were lower than those in the CCl_4-pbs group (Figure S2a-h; and S3a-h).

These findings indicate that mitochondrial function is dysregulated in the CCl_4-induced acute liver failure model. After MSC transplantation, mitochondrial function is regulated according to the degree of mitophagy activation in different cells. In hepatocytes, mitophagy is

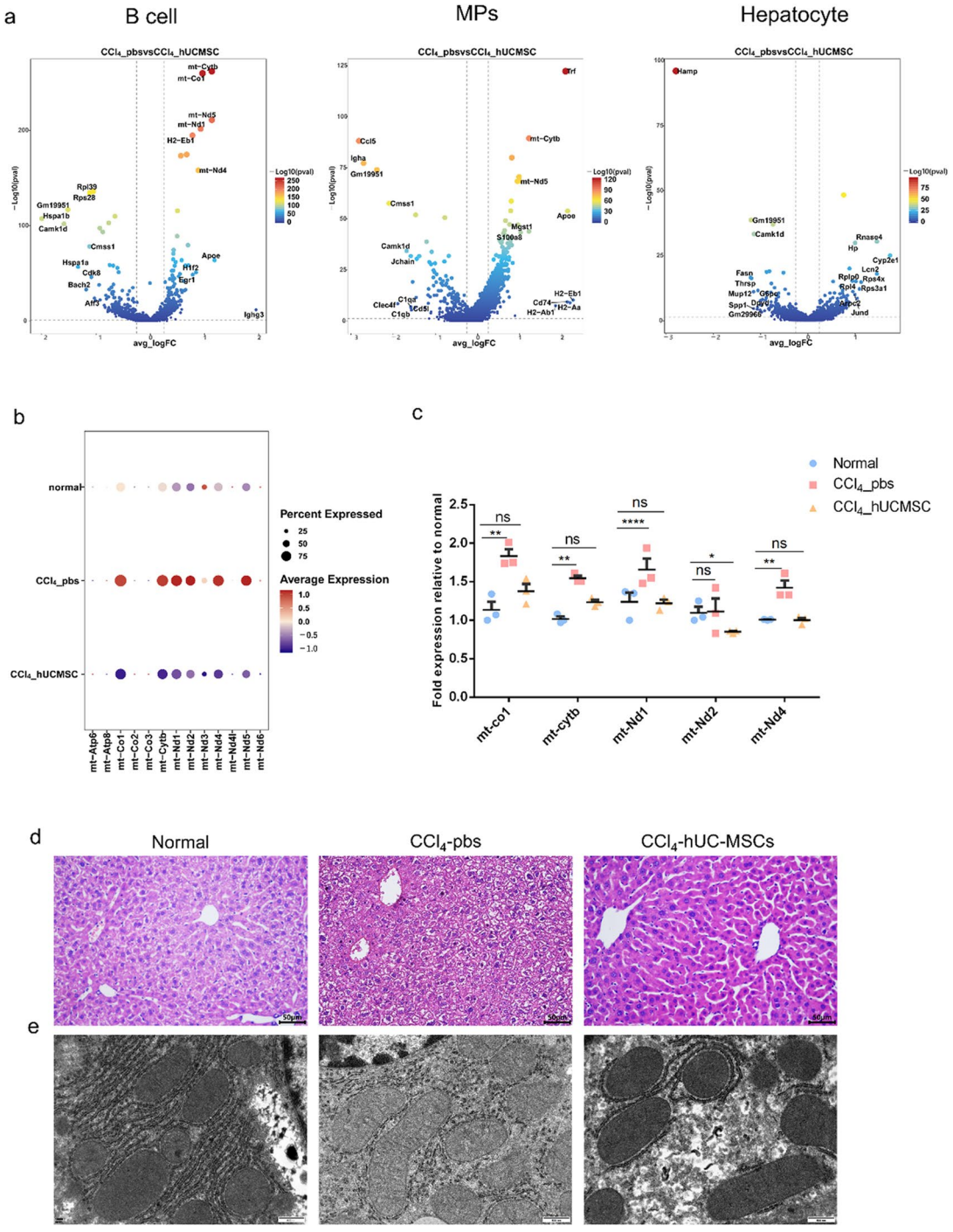

Fig. 2 Identification of differentially expressed mitochondria DNA based on single-cell RNA sequencing **(a)** Volcano plot of differentially expressed genes in each cell cluster. **(b)** Mitochondrial DNA expression levels in the normal, CCl_4-pbs and CCl_4-hUC-MSC groups. **(c)** qRT-PCR analysis of the expression of mitochondrial DNA. The animals were randomly divided into three groups ($n = 3$): the normal group, ALF group, and hUC-MSC transplantation group. C57BL/6J mice in the ALF group were injected with CCl_4 at a dose of 5 mL/kg body weight through intraperitoneal injection. Following CCl_4 treatment for 8 h, the animals were implanted with 1×10^6 hUC-MSCs through intraperitoneal injection. The ALF animals were treated with 300 μL of PBS. We harvested the liver tissue from the normal group and the CCl_4 group at 24 h, and the liver tissue from the hUC-MSC group was harvested at implantation day 7. **(d)** HE analysis. Scale bar = 50 μm. **(e)** Representative electron microscopy images of mitochondria from the normal group ($n = 3$), CCl_4-pbs group ($n = 3$) and CCl_4-hUCMSC group. Scale bar = 500 nm. Significance is indicated as $^*P < 0.05$, $^{**}P < 0.01$, $^{****}P < 0.0001$, and ns: not significant

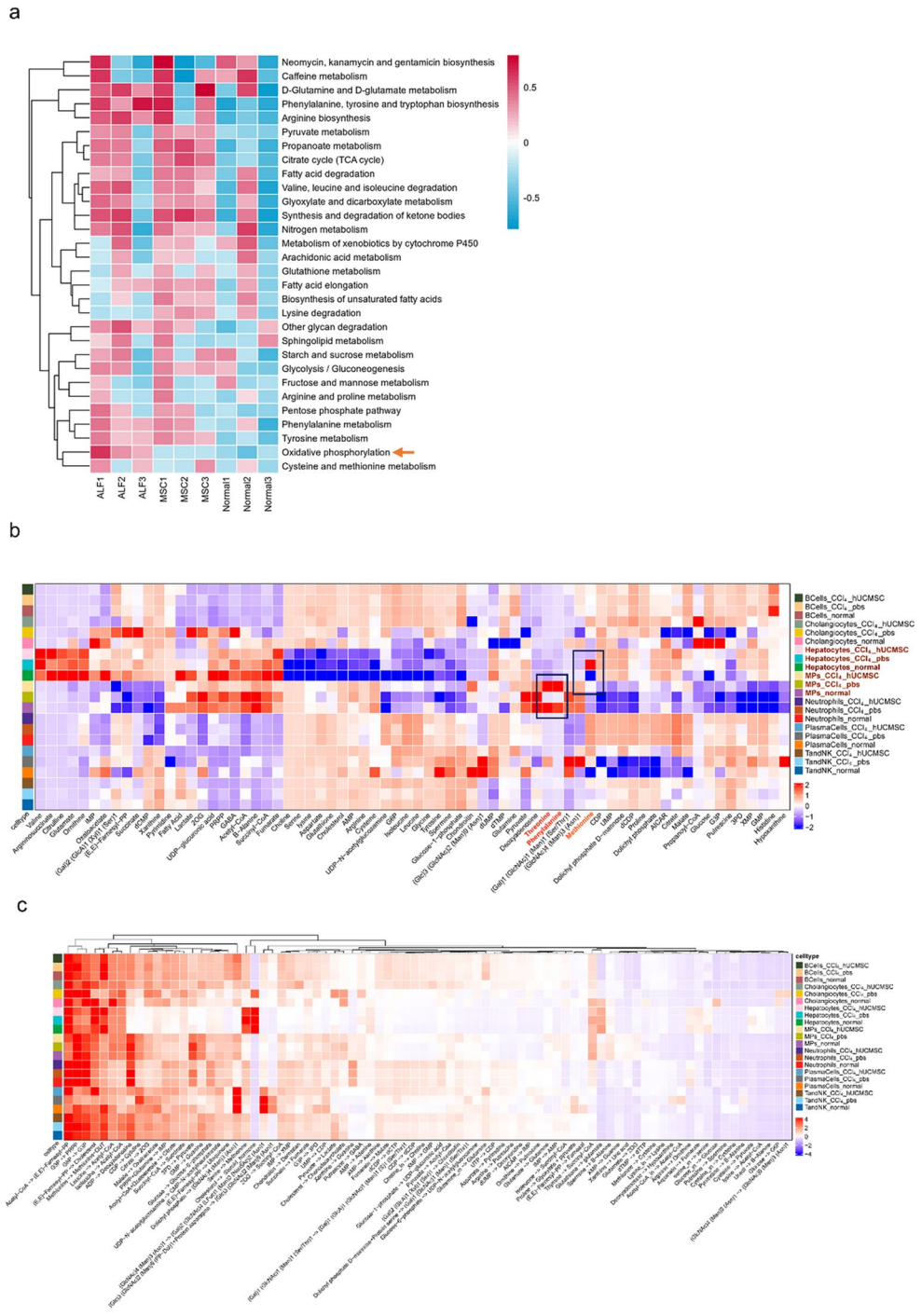

Fig. 3 scFEA estimate cell-wise metabolic flux using single cell RNA-seq data **(a)** Heat map of the metabolic pathways associated with the normal, CCl_4-pbs and CCl_4-hUCMSC groups determined using bulk RNA-seq. **(b)** Metabolite compounds of seven clusters. **(c)** Heat map of metabolic fluxes for different cell types in different metabolic modules

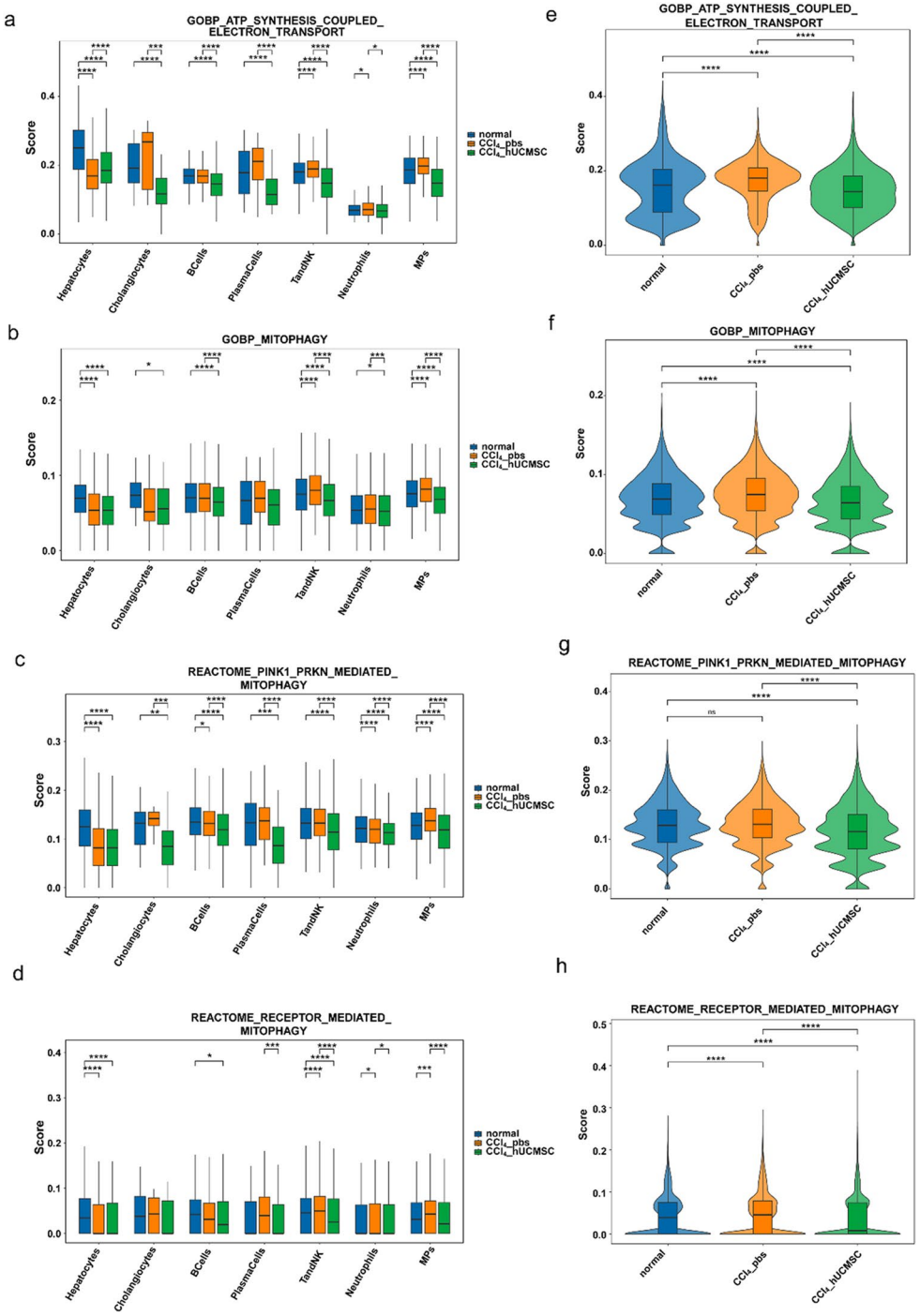

Fig. 4 Ucell score of mitochondria dysfunctional-related gene set in three group. **(a-d)** Ucell scoring of four mitochondria dysfunctional-related gene sets in hepatocytes, cholangiocytes, B cells, plasma cells, T cells, NKs, neutrophils and MPs. **(e-h)** Ucell scoring of the differences in the mitochondrial gene set scores among the three groups. Significance is indicated as $^{*}P < 0.05$, $^{**}P < 0.01$, $^{***}P < 0.001$, $^{****}P < 0.0001$, and ns: not significant

activated, whereas in other cell types, such as MPs, it is inhibited.

MSCs regulates the opposite expression patterns of mitophagy in hepatocytes and MPs of ALF mice

Mitophagy contributes to multiple pathological events and plays an important role in cell homeostasis. To examine the expression statuses of mitophagy-related genes in different cell types, we performed a differential gene analysis of the main cell clusters in the normal, ALF (CCl_4-pbs), and hUC-MSC transplantation groups. Based on these results, we conducted functional enrichment analysis and identified pathways related to mitochondrial autophagy, further revealing 30 mitochondria-related genes (MRGs) (Table S1).

An analysis of mitophagy genes in the MPs revealed that Slc25a5, Tspo, Gabarap, Becn1, Vps13c, and Bnip3L were significantly upregulated in the ALF (CCl_4-pbs) group (Fig. 5a). The expression of mitophagy receptors was also analyzed. Major receptors in the Ub-dependent (PINK1 and PRKN) and Ub-independent (Bnip3L/NIX, Bnip3, and Fundc1) mitophagy pathways were selected for correlation analyses. The data revealed markedly greater Bnip3L/NIX expression in the ALF (CCl_4-pbs) group than in the normal and hUC-MSC transplantation groups (Fig. 5b). qRT-PCR further confirmed that mitophagy genes (Beciln1, Tspo and Vps13c) and the mitophagy receptor Bnip3L/NIX were significantly upregulated in the ALF (CCl4-pbs) group compared with the hUC-MSC transplantation group (Fig. 5c).

An assessment of mitophagy-related genes in the hepatocytes suggested that Slc25a4, Fbxw7, Trp53 and Vps13d were relatively decreased in the ALF (CCl_4-pbs) group (Fig. 5a, Figure S4a, b). Interestingly, an analysis of mitochondrial receptors revealed that PINK1 and PRKN were strongly upregulated in the ALF (CCl_4-pbs) group compared with the normal and hUC-MSC transplantation groups (Fig. 5b, Figure S4c). We subsequently assessed the formation of autophagic vacuoles by TEM. As depicted in Fig. 5d, more autophagic vacuoles were detected in the ALF (CCl4-pbs) group than in the normal group, and hUC-MSC transplantation alleviated this effect. A GO enrichment analysis of hepatocytes revealed that compared with those in the CCl_4-hUCMSC group, pathways related to oxidative phosphorylation and mitochondrial electron transport chain complexes were significantly suppressed in the CCl_4-pbs group. Compared with those in the cells from liver injury model mice, functions such as oxidative phosphorylation, ATP metabolism, mitochondrial transport chain complex I, the NADH dehydrogenase complex, and the electron transport chain were significantly activated in hepatocytes from mice after hUC-MSC transplantation, thereby maintaining normal liver function and metabolic homeostasis (Fig. 6a, b).

Table 1 Primer used for real-time quantitative PCR

Gene	Sequence(5′→3′)
mt-Co1(F)	CTAACAGACCGCAACCTAAACAC
mt-Co1(R)	CCTACTGTGAATATGTGGTGGGC
mt-Cytb(F)	ACGCAAACGGAGCCTCAATA
mt-Cytb(R)	AAAGCGAAGAATCGGGTCAAG
mt-Nd1(F)	CATTGTTGGTCCATACGGCAT
mt-Nd1(R)	GGGTGTGGTATTGGTAGGGGA
mt-Nd2(F)	CCTATCACCCTTGCCATCATCT
mt-Nd2(R)	GCTGCTTCAGTTGATCGTGG
mt-Nd4(F)	TACTATAATCATGGCCCGAGGACT
mt-Nd4(R)	AAGGGCTATTAGTGTTAGTTCTCGTGT
Beclin1(F)	CCGTACAGGATGGACGTGGA
Beclin1(R)	TGGGTTTTGATGGAATAGGAGC
Arih1 (F)	ATTGAGAAGGATGGCGGTTGT
Arih1(R)	CTCCTCCATCTTCTGTTTCACC
Tspo(F)	TGGCCGATCTTCTGCTTGTC
Tspo(R)	GGCCCAATGGTCATAAAAGCA
Bnip3L/NIX(F)	GAAGATGGGCAGATCATGTTTG
Bnip3L/NIX(R)	CTGAAATGGAACTCTTTGGGTG
Vps13C(F)	CAAACCTTGCTTGCCACTTC
Vps13C(R)	AGAATGAATGACCTCAACTTGTGCT
Slc25a4(F)	GGCTGGTGTCCTATCCGTTT
Slc25a4(R)	GCGTTGGCTCCTTCATCTTT
Vps13d(F)	GTTACCAATCCTTCCCGTCCTT
Vps13d(R)	CCCAATAAATACTAAACTCAGCCAC
Fbxw7(F)	TTGATCCGTCTGATGACAGTAGC
Fbxw7(R)	AGACTTTGCATGGTTTCTTTCCC
Trp53(F)	CCCTCTGAGCCAGGAGACATT
Trp53(R)	CCCAGGTGGAAGCCATAGTTG
GAPDH(F)	CCTCGTCCCGTAGACAAAATG
GAPDH(R)	TGAGGTCAATGAAGGGGTCGT

MRGs enriched in specific MP subpopulations

To identify significantly expressed MRGs, we further intersected two gene sets. Set1 included 609 differentially expressed genes (DEGs) with significant differential expression in pairwise comparisons among the normal, ALF (CCl_4-pbs) and CCl_4-hUC-MSC transplantation groups (logFC > 0.20). Set 2 was the union set of MRGs from six mitophagy-related pathways, including 189 genes. Among them, six mitophagy-related pathways were obtained from the official Gene Set Enrichment Analysis (GSEA) website, with the corresponding accession numbers of GO:0000423, R-HSA-8,934,903, R-HSA-5,205,685, GO:0098779, GO:0000422 and GO:0042773 (Fig. 7a). The intersection of Set 1 and Set 2 resulted in the identification of 24 significantly expressed MRGs. Overall, these genes had positive correlations, with the above six mitochondrial genes showing the highest correlations (Fig. 7b). The expression of the 24 significantly expressed MRGs revealed that mitochondrial genes were highly expressed in all the main cell clusters except

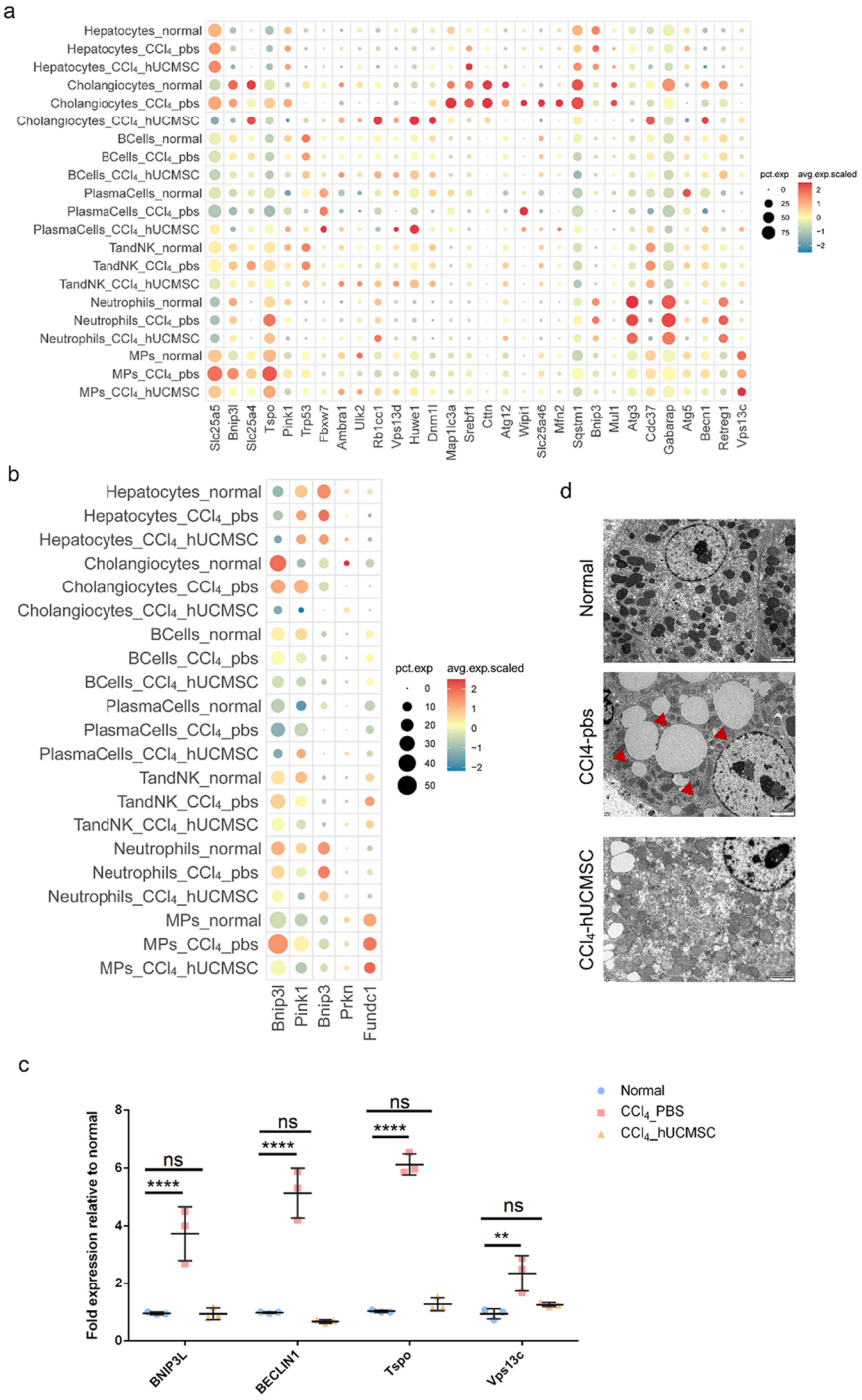

Fig. 5 Identification of mitophagy-related genes based on single-cell RNA sequencing **(a)** Dot plot of mitophagy-related genes in the normal group, ALF group and hUC-MSC transplantation group. **(b)** Dot plot of mitophagy receptor-related genes in the normal group, ALF group and hUC-MSC transplantation group.**(c)** qRT-PCR analysis of mitophagy-related gene expression in immune cells of the three groups. The animals were randomly divided into three groups ($n = 3$/group): a normal group, an ALF group, and an hUC-MSC transplantation group. The C57BL/6J mice in the ALF groups were injected with CCl_4 at a dose of 5 mL/kg body weight through intraperitoneal injection. After they were treated with CCl_4 for 8 h, the animals were implanted with 1×10^6 hUC-MSCs through intraperitoneal injection. The ALF animals were treated with 300 μL of PBS. We harvested the liver tissue from the normal group and the CCl_4 group at the time of CCl_4 treatment for 24 h, and the liver tissue from the hUC-MSC group was harvested at implantation day 7. And then immune cells were isolate for qRT-PCR analysis. Significance is indicated as $^{**}P < 0.01$, $^{****}P < 0.0001$, and ns: not significant. **(d)** Representative ultrastructural images of autophagic vacuoles (red arrows) in rat liver tissue. Scale bar = 2 μm

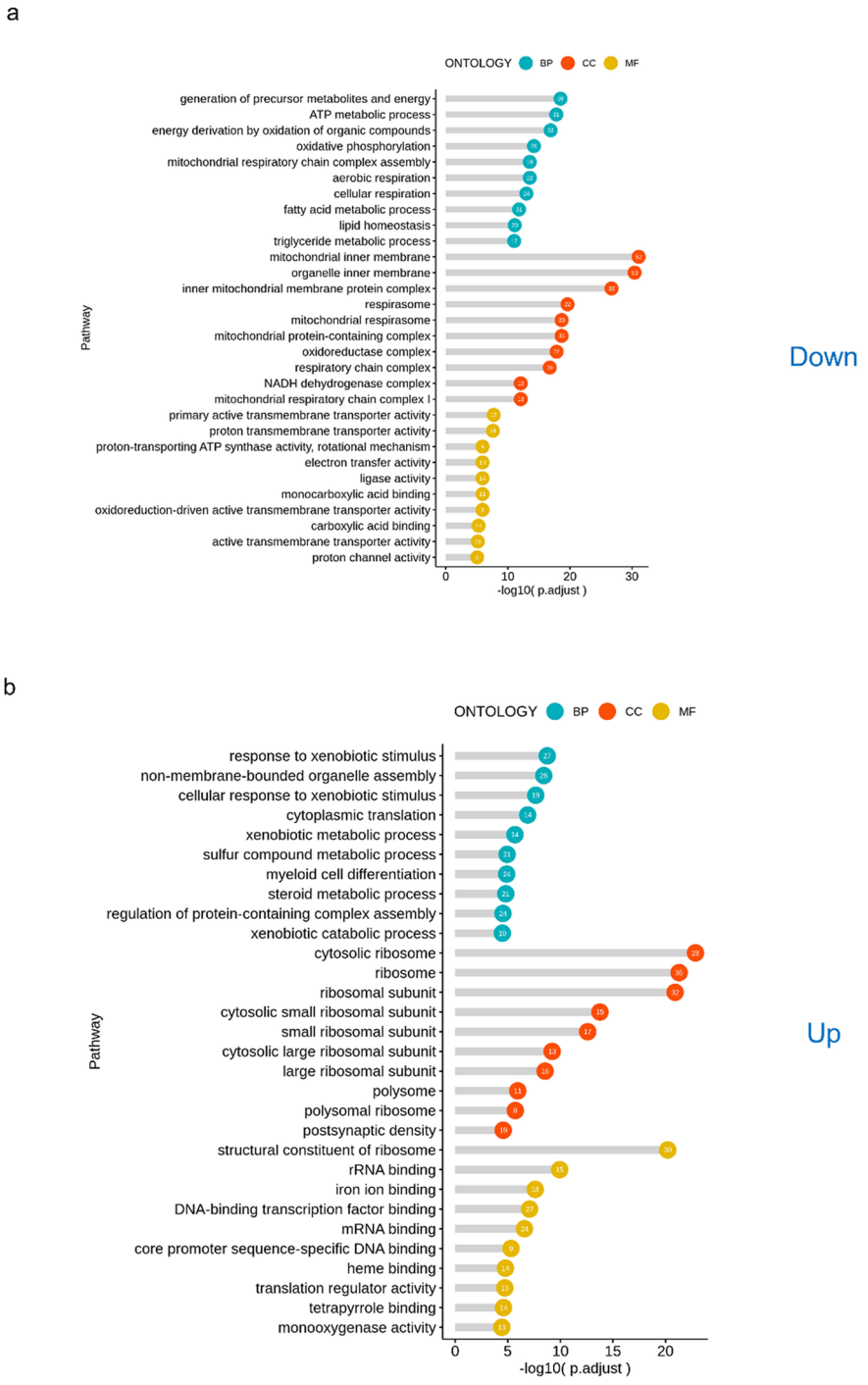

Fig. 6 Gene Ontology (GO) analysis of the DEGs in hepatocytes

neutrophils, and Cox8, Ubb, Tspo, Bnip3l and Slc25a5 were the most prominent (Figure S5 a-x).

We further subdivided and annotated MP cells into seven different subtypes (Fig. 7c), including macrophages (C1qa + C1qb + C1qc+), classical monocytes (Ly6c2 + Ccr2 + Sell+), nonclassical monocytes (Ace + Ear2 + Cx3cr1 + Eno3+), cDC1s (Xcr1 + Clec9a+), cDC2s (Cd209a + Clec10a+), pDCs (Siglech + Ccr9+), and Kupffer cells (Clec4f + Cd5l + Vsig4 + Timd4 + Marco +) (Fig. 7d). The expression of 24 differentially expressed mitochondria-related genes (DE-MRGs) was subsequently analyzed in different MP-containing cells. The results revealed that MRGs were enriched in macrophage subpopulations (Figure S6a-x). Among the genes examined here, Bnip3L, Slc25a4, Tspo, Atg5, Retreg1 and

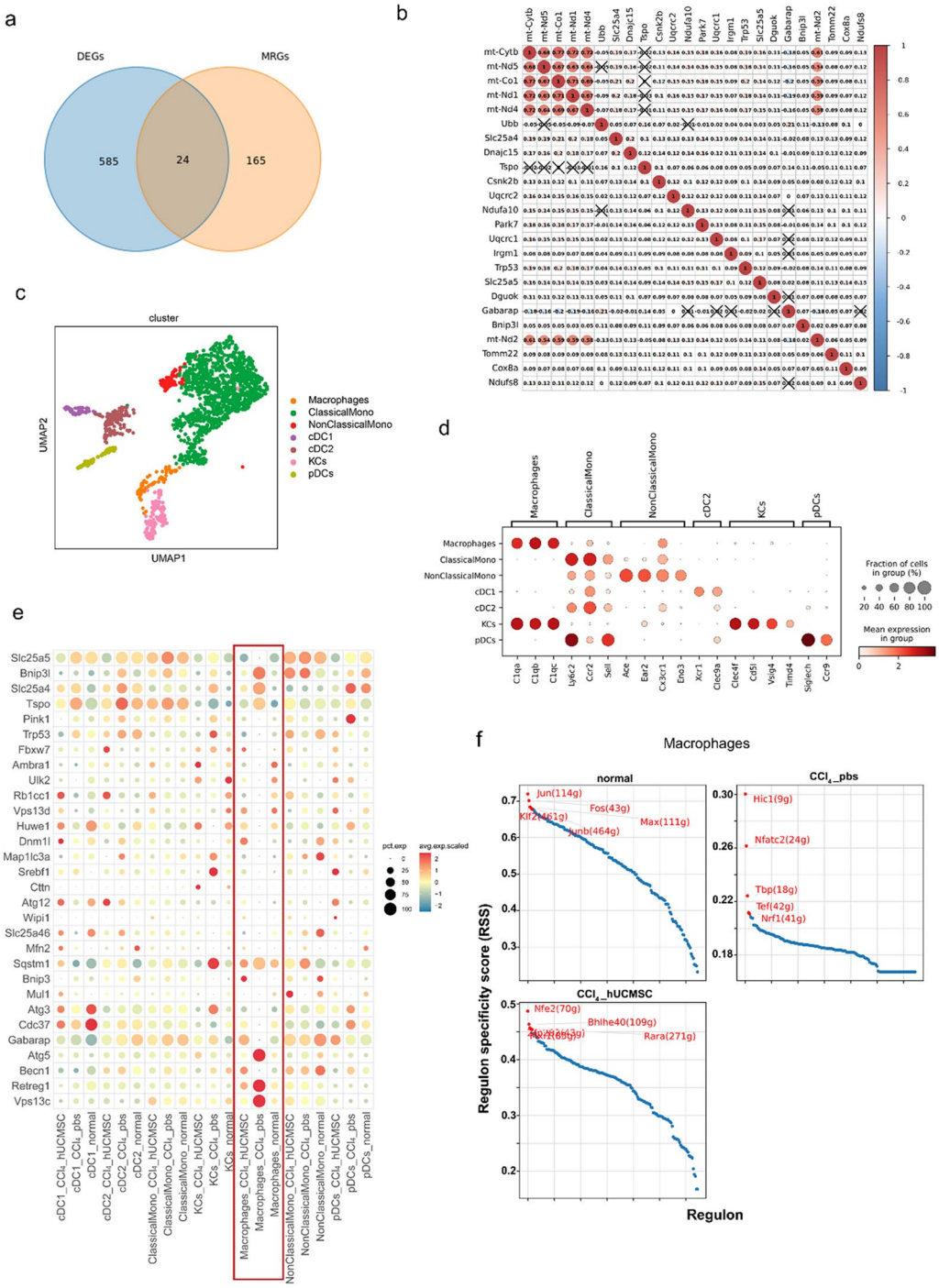

Fig. 7 Identification of differentially expressed mitophagy-related genes based on single-cell RNA sequencing. **(a)** Venn diagram analysis of DE-MRGs between cell markers and MRGs. **(b)** Correlation analysis of 24 DE-MRGs. The numbers represent the correlations between 24 DE-MRGs; X represents significance. **(c)** UMAP plots of 7 MP cell subpopulations in ALF. **(d)** Dot plots showing the expression of cell markers in 7 cell subpopulations. **(e)** Dot plots showing the DE-MRGs in 7 cell subpopulations of MPs. **(f)** SCENIC analysis of transcription factors in the macrophage cluster

VPS13c were the most significantly enriched in the macrophage subpopulations (Fig. 7e).

Next, SCENIC analysis was conducted to explore the regulatory mechanisms underlying the gene expression patterns detected in the above macrophage subpopulations (Figure S7). Specifically, the modulatory roles of transcription factors in macrophages were examined in mice with experimental ALF. The activities of the following transcription factors were specifically elevated in the macrophage subpopulations in the CCl_4-pbs

group: Nrf1 (41 g), Hic1 (19 g), Nfatc2 (24 g), Tbp (18 g), and Tef (42 g) (Fig. 7f). The above data provide novel insights for an in-depth understanding of the modulatory mechanisms by which transcription factors control mitochondrial metabolism in macrophages.

hUC-MSCs transplantation induced the expression of the ubiquitin ligase Arih1

To identify the specific transcriptomic changes of MPs after hUC-MSCs treatment, we analyzed the DEGs among three groups. Differential gene enrichment analysis revealed that, compared with those in the CCl_4-hUCMSC group, pathways related to mitochondrial dysfunction, such as apoptosis-induced mitochondrial changes, changes in the mitochondrial membrane potential, and autophagy, were significantly activated in the CCl4-pbs group; similarly, molecular functional pathways related to ubiquitin protein ligase binding were also significantly activated (Fig. 8a). In general, cellular components related to cell apoptosis and mitochondrial dysfunction, i.e., autophagosomes and secondary lysosomes, were significantly enriched in the hepatocytes of liver injury model mice. The results of the differential gene enrichment analysis revealed that the biological processes related to ubiquitin-protein ligases were significantly enriched. We intersected the 43 significantly enriched pathway genes related to ubiquitin-protein ligases or transferases to obtain 19 key ubiquitin ligase genes and assessed their expression in major cell types of different groups. The results revealed that the E3 ubiquitin ligase Arih1 significantly increased after hUC-MSC transplantation, especially in MPs and T, NK, and B cells (Fig. 8b, c).

Discussion

The major factor causing ALF is immense hepatocyte necrosis upon liver injury, the physiological processes of which are very complex. However, increasing evidence suggests that ALF is associated with strong systemic inflammation and immune dysfunction [22, 23]. Previous findings have suggested that after the selective elimination of damaged or excess mitochondria, mitophagy maintains mitochondrial homeostasis, inhibits the release of proinflammatory cytokines induced by the NLR family pyrin domain-containing protein 3 (NLRP3) inflammasome, and decreases the local inflammatory response and tissue necrosis [24, 25]. During the development of ALF, the mitochondria in damaged hepatocytes release damage-associated molecular patterns and secrete the inflammatory cytokines IL-1β and TNFα; additionally, reactive oxygen species (ROS) are elevated, ATP depletion occurs, serine/threonine-protein kinase (mTOR) activity is suppressed, and autophagy is increased. Excess autophagosomes accumulate around necrotic foci, limiting the expansion of necrotic areas to relatively normal areas of the liver. By translocating to the mitochondria or ubiquitinating mitochondrial proteins, mitophagy-associated proteins induce mitophagy to help clear damaged mitochondria and ROS while decreasing the inflammatory response and contributing to the repair of injured hepatocytes [26].

Recent evidence suggests that at disease onset, mitophagy activation is not sufficient to help remove damaged mitochondria in a timely manner, resulting in the hindered repair of necrotic hepatocytes, thereby exacerbating local and systemic inflammation and eventually leading to irreparable and massive necrosis of the liver parenchyma [14]. During the process of drug-induced ALF caused by acetaminophen (APAP), targeted inhibition/knockdown of the Parkin protein significantly inhibits mitophagy, leading to the accumulation of the NLRP3 inflammasome and exacerbating APAP-induced hepatotoxicity [27]. Mitophagy induction removes mitochondria damaged by ROS, inhibits IL-1β secretion, and alleviates APAP-induced ALF [28]. These findings suggest a crucial role for mitophagy in liver tissue protection to maintain liver homeostasis; conversely, mitophagy suppression induces the accumulation of damaged mitochondria in the liver, disrupting the homeostatic environment of mitochondria and exacerbating ALF development [15].

However, a recent study revealed that mice with pathogenic mutations in FBXL4 exhibit defective degradation of BNIP3 and Bnip3L/NIX, resulting in excessive mitophagy activation. Therefore, mitophagy overactivation might represent a critical pathogenic mechanism and lethal event in human pathologies [16]. Furthermore, Zhao and colleagues reported that the level of mitophagy is significantly increased in alcoholic liver disease and that pretreatment with fucoidan can prevent ethanol-induced accumulation of damaged mitochondria and excessive activation of mitophagy, thus maintaining mitochondrial homeostasis and ensuring mitochondrial quality [29]. Consequently, overactive mitophagy is a potential target for regulating disease occurrence. However, whether excessive mitophagy is involved in the development of ALF remains undefined. Therefore, a few questions are worth asking. In ALF, does excessively active mitophagy actually occur? Which cell types mediate this overly active mitophagy? Do different cell subtypes display distinct mitophagy states? To address these questions, single-cell sequencing was employed to analyse the mitophagy levels of various cell subsets in the livers of ALF and hUC-MSC-transplanted mice, and exciting outcomes were achieved.

An ideal animal model may play a pivotal role in recapitulating disease features and unravelling the underlying pathogenic mechanisms of diseases. Within the past decade, researchers have developed a series of animal

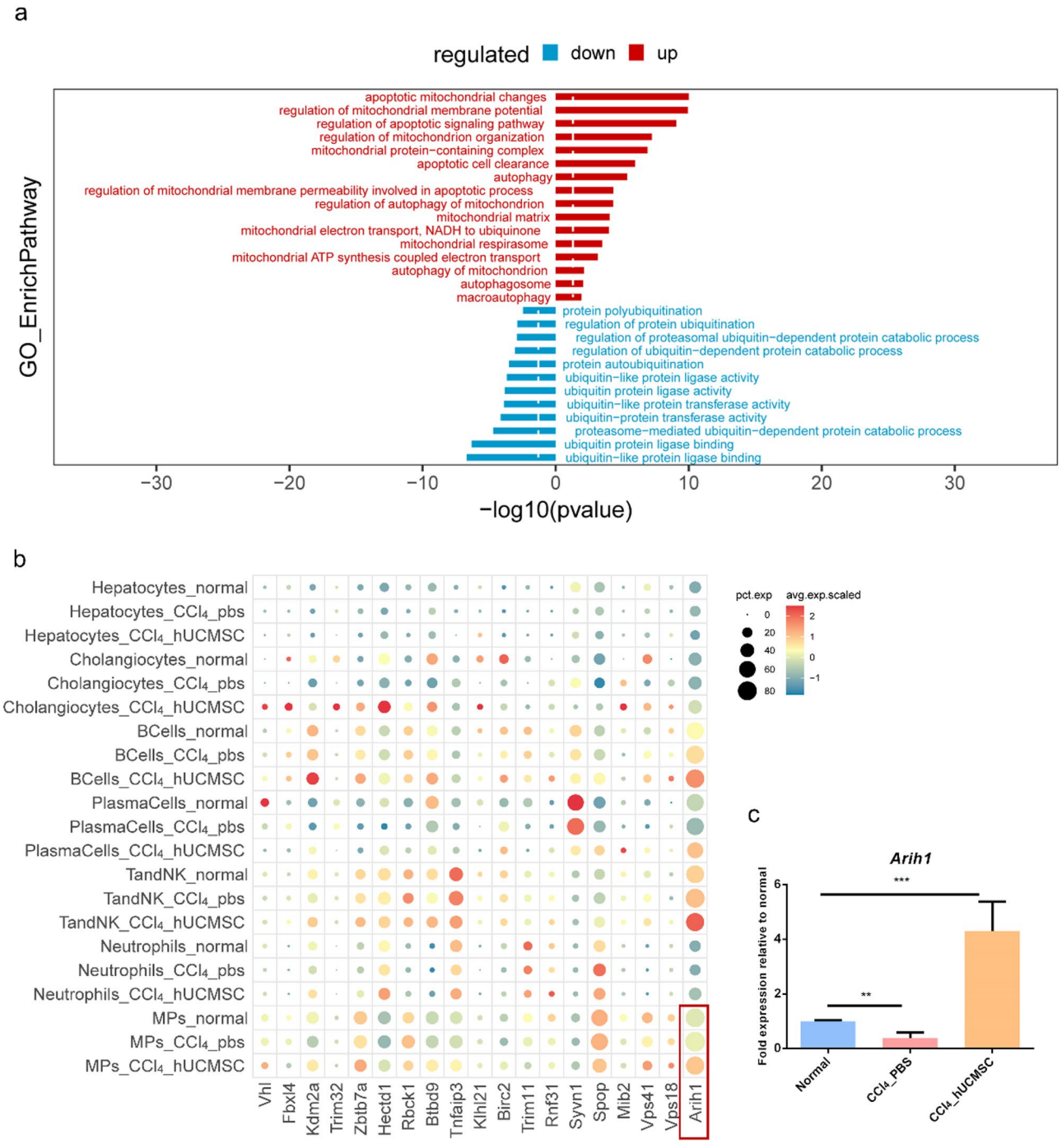

Fig. 8 Gene ontology (GO) analysis **(a)** Gene Ontology (GO) analysis of the downregulated pathways and upregulated pathways of the DEGs associated with MPs. **(b)** The 19 ubiquitin protein ligases expressed in the three groups. **(c)** qRT-PCR analysis of *Arih1* expression in immune cells of the three groups. Significance is indicated as $^{**}P < 0.01$, $^{***}P < 0.001$

models using various CCl_4 doses, including lethal doses, for the study of liver injury. To simulate ALF symptoms as accurately as possible, we initially monitored the survival rate, liver function indices, and pathological features of mice that were intraperitoneally injected with different doses of CCl_4. On the basis of these comprehensive observations, we ultimately determined that a 5 ml/kg dose of CCl_4 would be suitable for constructing the ALF model. Single-cell transcriptome sequencing combined with bulk RNA analysis revealed an inhibitory effect on mitophagy in hepatocytes, which is mediated by the classical ubiquitin (Ub)-dependent PINK1 mitophagy pathway. This phenomenon manifests primarily as decreased PINK1 expression, obstructed energy metabolism

pathways, such as the oxidative phosphorylation pathway, and impaired methionine metabolism. These actions may have occurred because during ALF occurrence, hepatocytes are typically confronted with severe stress and damage inducers, e.g., oxidative stress and inflammatory responses [30]. The influx of numerous damage-related signals into hepatocytes disrupts or dysregulates key nodes within autophagy-associated signaling pathways. For example, the abnormal activation of mTOR often leads to autophagy inhibition, thereby leaving damaged mitochondria lingering in the cells without timely clearance. This situation not only undermines the normal functions of hepatocytes but also jeopardizes their survival, ultimately leading to more severe liver injury [31].

However, in the MPs of the ALF mouse model (ALF-MPs), mitophagy was found to be overactive. This overactive mitophagy is mediated by Bnip3L/NIX, a mitophagy receptor in the non-Ub-dependent pathway. Current evidence suggests that, as a key immune component, MPs infiltrate liver tissue after liver injury, mediating immune surveillance as well as the clearance of pathogens and damaged cells [32]. Enhanced mitophagy helps MPs maintain normal mitochondrial function and metabolic status, providing sufficient energy and a stable internal environment for the execution of their immune functions [33]. Nevertheless, mitophagy activation within cells has a definite upper limit, and surpassing this threshold may trigger tissue or organ degeneration.

MSCs have shown marked efficacy in animal ALF models and a few human studies, and their potential therapeutic mechanism may involve the regulation of the immune function and the attenuation of the inflammatory response through the secretion of soluble factors and cellular communication [34–38]. Liao et al. reported that in metabolic diseases, MSCs improve mitochondrial dysfunction through Pink1/Parkin-mediated mitochondrial autophagy, thereby protecting endothelial cells from hyperglycaemia-induced damage [39]. Therefore, MSCs likely inhibit the inflammatory response and attenuate ALF progression via the mitochondrial autophagy pathway. TEM revealed that the mitochondrial structure was clearer, with regularly arranged cristae, in the hUC-MSC-transplanted mice than in the ALF model mice, suggesting that hUC-MSC transplantation indeed repaired the mitochondrial structure. Furthermore, the expression of the mitochondrial genes mt-co1, mt-cytb, mt-Nd1, mt-Nd2, and mt-Nd4 was abnormal in mice with CCl_4-induced ALF, and the MPG Beclin1 gene was upregulated. These levels were similar to those of normal mice after hUC-MSC transplantation, which is consistent with the TEM results for mitochondrial structure. Moreover, Ucell scoring indicated that the ATP-coupled electron transport pathway and mitophagy pathway gene sets in liver samples from hUC-MSC-transplanted mice were closely related to those in liver samples from normal mice. The scores were highest in samples from the CCl_4-pbs-induced liver injury model, indicating that mitochondrial homeostasis was restored to normal levels after hUC-MSC transplantation. These findings indicate that after hUC-MSC transplantation, mitophagy is activated in hepatocytes and inhibited in macrophages, with the mitochondrial homeostasis environment returning to normal levels after hUC-MSC transplantation. DEG GO enrichment analysis revealed that molecular functional pathways related to ubiquitin ligase binding were activated to different degrees. On this basis, we selected the ubiquitin ligase gene set and DEGs for intersection gene analysis and found that the expression of the E3 ubiquitin ligase Arih1 was significantly upregulated after hUC-MSC transplantation in the MP subset. Therefore, we speculate that hUC-MSCs may degrade the mitophagy receptor Bnip3L/NIX through the ubiquitin ligase Arih1, suppress mitophagy, maintain mitochondrial homeostasis, exert immunoregulatory effects, and eventually promote liver repair. However, the mechanism by which Arih1 degrades Bnip3L/NIX and suppresses mitophagy through ubiquitination during the occurrence and development of ALF remains to be further studied.

Conclusions

We successfully identified a trend in an ALF mouse model in which mitophagy in hepatocytes and MPs exhibited opposite patterns. This phenomenon reflects the distinct strategies adopted by different cell types to adapt to the environment and maintain their respective functions in the context of the pathological state of acute liver failure. These findings also suggest that targeting mitophagy in different cell types may be a potential strategy for ALF treatment. Therefore, this study not only reveals the dynamic changes in mitophagy in different cells during ALF but also, surprisingly, reveals the distinct mechanisms of action of MSC transplantation in parenchymal and immune cells. These findings provide new theoretical and experimental evidence for treating ALF with MSCs.

Methods

Animal experiments

Laboratory animals

A total of 60 C57BL/6J mice (weighing 16–18 g, aged 6–8 weeks) were purchased from Spiff Biotechnology Company and maintained on 12 h light/dark cycles with food and water available at the Laboratory of Ningxia Medical University. For each independent experiment, the mice were anaesthetized with 5% pentobarbital sodium (5 mg/kg). All the animals were treated in accordance with the principles of the Declaration of ARRIVE guidelines and EU Directive 2010/63/EU on the protection of animals

used for scientific purposes. The animal procedures described here were reviewed and approved by the Ethics Committee of the General Hospital of Ningxia Medical University (NO. KYLL-2024-0978).

Inclusion and exclusion criteria

The animals were included in the study if they received successful CCl_4 intraperitoneal injection, as defined by inflammatory cells infiltrating the stroma through haematoxylin-eosin staining. The animals were excluded from this study if they received no cell therapy and survived for 72 h, preventing the collection of behavioural and histological data.

Blinding/Masking

For each animal, four different researchers participated in the experiment. The first investigator administered the treatment according to the randomization table. The second investigator was responsible for the anaesthetic procedure. The third investigator performed the CCl_4 intraperitoneal injection. The fourth investigator performed the cell transplantation.

Experimental grouping and intervention method

The animals were randomly divided into three groups ($n = 20$/group): a normal group, an ALF group, and an hUC-MSC transplantation group. The C57BL/6J mice in the ALF groups were intraperitoneally injected with CCl_4 at a dose of 5 mL/kg body weight. Following treatment with CCl_4 for 8 h, the animals were implanted with 1×10^6 hUC-MSCs through intravenous injection. The animals in the ALF group were treated with 300 μL of PBS.

Histopathology

Seven days after the injection of hUC-MSCs, the mice were euthanized with pentobarbital, and their liver tissues were isolated and fixed with 10% formalin. The fixed livers were then embedded in paraffin wax. Five-micrometre-thick sections were prepared for haematoxylin and eosin (H&E) staining and Masson staining.

Analysis of pro-inflammatory factor by ELISAs

The weight of the liver tissue was precisely measured. Subsequently, homogenization medium (0.9% saline) was added at a volume 9 times greater than the tissue weight, at a weight (mg)-to-volume (μl) ratio of 1:9. The mixture was then mechanically homogenized in an ice-water bath to prepare a 10% homogenate. Afterwards, the homogenate was centrifuged at 3000 rpm for 10 min. Lastly, the supernatant was carefully collected for the subsequent assay. The levels of IL-1β, TNF-α and IL-6 in liver tissue from animals treated with various doses of CCl_4 were determined using ELISA with kits from Invitrogen (Cat No. 88-7064-88, Cat No. 88–7013 A-88, Cat No. 88-7324-88) according to the manufacturer's instructions.

Animal survival and biochemical analysis

Six mice in each group were used for the survival analysis. The survival of the CCl_4-induced ALF mice at doses of 0 ml/kg, 2.5 ml/kg, 5 ml/kg, 6 ml/kg, 7 ml/kg and 10 ml/kg was assessed. Serum samples were obtained by centrifugation within 1 h of collection and were used to detect the specific markers of liver injury, including albumin (ALB), alanine transaminase (ALT), aspartate transaminase (AST), total bilirubin (TBiL) and total bile acid (TBA) bilirubin, after intraperitoneal injection of CCl_4 at doses of 2.5 ml/kg, 5 ml/kg, and 7 ml/kg for 24 h.

TEM

At the end of each treatment, liver tissue was harvested within 3 min and washed with PBS three times. The samples were sequentially fixed in 2.5% glutaraldehyde and 1% osmium tetroxide on ice for 1 h and washed three times with 0.1 M cacodylate buffer containing 0.1% $CaCl_2$. Then, the samples were embedded in an Epon 812 mixture and polymerized in an oven at 60 ℃ for 36 h. Using an Ultracut UC7 ultramicrotome (Leica, Austria), 70-nm-thick sections were cut and mounted on 75-mesh copper grids. The sections were counterstained with uranyl acetate for 10 min followed by lead citrate for 7 min and then examined with KBSI BioHigh Voltage EM (JEM-1400 at 120 kV and JEM-1000BEF at 1000 kV; JEOL, Ltd., Tokyo, Japan).

Immune cells isolation

The mouse livers were infused through the portal veins with 15 mL of PBS for 2 min at 4 ℃. Then, the livers were cut into small fragments, which were mixed with dissociation enzymes (Miltenyi Biotec, Bergisch Gladbach, Germany) in gentleMACS C tubes (Miltenyi Biotec) and homogenized with a GentleMACS™ Dissociator (Miltenyi Biotec). The digested livers were filtered using 70 μm cell strainers and washed with 5 mL of Dulbecco's modified Eagle's medium (DMEM). Single cells were resuspended in 40% Percoll (GE Healthcare) and centrifuged at 600 ×g for 5 min, followed by red cell lysis with ACK lysis buffer (Gibco) to lyse the red blood cells. The cell suspensions were harvested for qRT-PCR experiments.

qRT-PCR

A QIAzol lysis reagent and an RNeasy Kit (Qiagen, CA, USA) were used to extract total RNA from the liver tissues according to the manufacturer's protocols. The RNA samples were quantified using a NanoDrop 2000 system (Thermo Scientific, USA). cDNA was synthesized from 0.2 μg of RNA using the PrimeScript™ RT reagent kit and gDNA Eraser (Perfect Real Time) (Takara, Beijing).

cDNA (1 μl) was subsequently amplified by fluorescent quantitative real-time PCR (qRT-PCR) using TB Green® Premix Ex Taq™ II and an ABI Prism 7500 Sequence detection system (Applied Biosystems, USA). For the immune cells, RNA was extracted using the RNeasy Micro Plus Kit (Qiagen) according to the manufacturer's instructions, and 10 ng of RNA was reverse transcribed and amplified using the Whole Transcriptome Kit (Qiagen).

The levels of the target genes were normalized to the level of GAPDH, which was used as an endogenous control, and the relative gene expression was calculated using the $2^{-\Delta\Delta Ct}$ method. The primer sequences are provided in Table 1. All the data are presented as the means of three independent experiments.

ScRNA sequencing

Single-cell preparation

Normal mice, ALF mice and hUC-MSC-implanted mice were prepared, and liver tissues were collected for single-cell RNA-seq. The liver tissues were stored in sCellLive™ Tissue Preservation Solution (Singleron Biotechnologies, Nanjing, China). Singleron PythoNTM Automated Tissue Dissociator (Singleron Biotechnologies) and sCelLive TM Tissue Dissociation Mix (Singleron Biotechnologies) were used to prepare single-cell suspensions from liver samples.

Single-cell RNA sequencing

Single-cell suspensions (1×10^5 cells/mL) were prepared and loaded onto microfluidic devices to generate scRNA-seq libraries according to the Singleron GEXSCOPE® protocol [40]. Individual libraries were diluted to 4 ng/μL and pooled for sequencing on an Illumina HiSeq X (Illumina, San Diego, CA, USA).

Single-cell RNA statistical analysis

The raw reads were processed through fastQC v0.11.4 to generate fastp to filter the adaptor sequence, and low-quality reads were removed to obtain clean data. Scanpy v1.8.1 was used for quality control. We filtered low-quality cells that contained fewer than 200 expressed genes, cells with the top 2% of the UMI count and cells with a mitochondrial content > 5%. Following filtration, 25193 cells with an average of 1043.3 genes and 2362.8 UMIs per cell were retained for downstream analyses. The raw count matrix was normalized by total counts per cell and logarithmically transformed into a normalized data matrix, and the top 2000 variable genes were selected by setting the flavour='seurat' for principal component analysis (PCA). The top 20 principal components were selected for clustering and dimensionality reduction, and the cells were separated into 23 clusters using the Louvain algorithm, which was based on setting the resolution parameter at 1.2. Uniform manifold approximation and projection (UMAP) was used to visualize the target cell clusters. We selected the top 20 differentially expressed genes in each cluster. We used hypergeometric tests (HGTs) to annotate our single-cell RNA-seq data [41].

Differentially expressed gene (DEG) analysis

To identify the DEGs among the three samples, the Scanpy.tl.rank gene group function based on the Wilcoxon rank sum test with default parameters was used according to the following criteria: fold change > 0.25 and p value < 0.05.

GO and KEGG analysis of DEGs

The "clusterProfiler" R package v 3.16.1 was used for Gene Ontology (GO) and Kyoto Encyclopedia of Genes and Genomes (KEGG) analyses. Pathways with $p < 0.05$ were identified as significantly enriched and are plotted as bar plots.

UCell gene set scoring

Five-mitochondrion gene set scoring among different cell clusters and samples was performed using the R package UCell v 1.1.0. UCell scores are based on the Mann-Whitney U statistic by ranking query genes in order of their expression levels in individual cells [42].

Gene regulatory network inference

We employed SCENIC (version 1.1.0) with default parameters to analyse the enrichment of transcriptome factors in MPs. For SCENIC, the input matrices for each individual sample were the raw UMI counts obtained from Seurat.

Evaluation of metabolic activity

We used scFEA to assess metabolite abundance based on scRNA-seq data. Additionally, we employed gene set variation analysis (GSVA) to compute the enrichment score of each metabolic pathway in every sample using transcriptomic data.

Abbreviations

ALF	Acute liver failure
hUC-MSCs	Human umbilical cord mesenchymal stem/stromal cells
ALB	Alumin
CCl_4	Carbon tetrachloride
MRGs	mitophagy-related genes
MPs	mononuclear phagocytes
GO	Gene Ontology
KEGG	Kyoto Encyclopedia of Genes and Genomes

Supplementary Information

The online version contains supplementary material available at https://doi.org/10.1186/s13287-025-04491-3.

Supplementary Material 1

Acknowledgements
The authors declare that they have not use AI-generated work in this manuscript.

Author contributions
Sang Luo and Fang Wu conducted all the experiments and data analysis. Sang Luo conceived the idea and supervised the entire project, including manuscript preparation and revision. Xiaojun Yang provided administrative support. All authors read and approved the final manuscript.

Funding
This work was supported by grants from Special Talent Introduction Project of Ningxia Autonomous Region Key R&D Programs (NO. 2024BEH04106); Science and Technology Support Project of Yinchuan City (No.2024SF045).

Data availability
The data supporting this study's findings are available from the corresponding author upon reasonable request. Single-cell RNA sequencing data of mouse liver were provided in Sequence Read Archive (NO. PRJNA1137063, https://www.ncbi.nlm.nih.gov/bioproject/PRJNA1137063.)

Declarations

Ethics approval for animals
This study was reviewed and approved by the Ethics Committee of General hospital of Ningxia Medical University [1] Title of the approved project: Mechanistic study of autophagy inhibition by Arih1 through ubiquitination degradation of NIX [2]. Name of the institutional approval committee: Ethics Committee of General hospital of Ningxia Medical University [3]. Approval number: NO. KYLL-2024-0978 [4]. Data of approval: 4 June 2024.

Human Ethics approval and consent to participate
This study contains no patient(s) or their guardian(s) participation.

Competing interests
The authors declare no competing interests.

Received: 15 May 2025 / Accepted: 30 June 2025
Published online: 06 July 2025

References

1. Wang C, et al. Macrophage polarization and its role in liver disease. Front Immunol. 2021;12. https://doi.org/10.3389/fimmu.2021.803037.
2. Lemmer P, Sowa JP, Bulut Y, Strnad P, Canbay A. Mechanisms and aetiology-dependent treatment of acute liver failure. Liver Int. 2023. https://doi.org/10.1111/liv.15739.
3. Balvey A, Fernandez M. Translational control in liver disease. Front Physiol. 2021;12. https://doi.org/10.3389/fphys.2021.795298.
4. Kamar N, et al. Hepat E Lancet. 2012;379:2477–88. https://doi.org/10.1016/s0140-6736(11)61849-7.
5. Khuroo MS, Kamili S. Aetiology and prognostic factors in acute liver failure in India. J Viral Hepatitis. 2003;10:224–31. https://doi.org/10.1046/j.1365-2893.
6. Torres HA, Davila M. Reactivation of hepatitis B virus and hepatitis C virus in patients with cancer. Nat Reviews Clin Oncol. 2012;9:156–66. https://doi.org/10.1038/nrclinonc.2012.1.
7. Zhao P, et al. Causes and outcomes of acute liver failure in China. PLoS ONE. 2013;8:e80991. https://doi.org/10.1371/journal.pone.0080991.
8. Innokentev A, Kanki T. Mitophagy in yeast: molecular mechanism and regulation. Cells. 2021;10. https://doi.org/10.3390/cells10123569.
9. Scheibye-Knudsen M, Fang EF, Croteau DL, Wilson DM, Bohr VA. Protecting the mitochondrial powerhouse. Trends Cell Biol. 2015;25:158–70.
10. Peoples JN, Saraf A, Ghazal N, Pham TT, Kwong JQ. Mitochondrial dysfunction and oxidative stress in heart disease. Exp Mol Med. 2019;51:1–13. https://doi.org/10.1038/s12276-019-0355-7.
11. Bock FJ, Tait SWG. Mitochondria as multifaceted regulators of cell death. Nat Rev Mol Cell Biol. 2019;21:85–100. https://doi.org/10.1038/s41580-019-0173-8.
12. Rong Z, et al. The mitochondrial response to DNA damage. Front Cell Dev Biology. 2021;9. https://doi.org/10.3389/fcell.2021.669379.
13. Wang H, Zheng Y, Huang J, Li J. Mitophagy in antiviral immunity. Front Cell Dev Biol. 2021;9:723108. https://doi.org/10.3389/fcell.2021.723108.
14. Lu X, et al. AMPK protects against alcohol-induced liver injury through UQCRC2 to up-regulate mitophagy. Autophagy. 2021;17:3622–43. https://doi.org/10.1080/15548627.2021.1886829.
15. Zhang IW, et al. Mitochondrial dysfunction governs immunometabolism in leukocytes of patients with acute-on-chronic liver failure. J Hepatol. 2022;76:93–106. https://doi.org/10.1016/j.jhep.2021.08.009.
16. Cao Y, et al. A mitochondrial SCF-FBXL4 ubiquitin E3 ligase complex degrades BNIP3 and NIX to restrain mitophagy and prevent mitochondrial disease. EMBO J. 2023;42:e113033. https://doi.org/10.15252/embj.2022113033.
17. Bernal W, et al. Lessons from look-back in acute liver failure? A single centre experience of 3300 patients. J Hepatol. 2013;59:74–80. https://doi.org/10.1016/j.jhep.2013.02.010.
18. Stravitz RT, Lee WM. Acute liver failure. Lancet. 2019;394:869–81. https://doi.org/10.1016/S0140-6736(19)31894-X.
19. Kwong AJ, et al. OPTN/SRTR 2022 Annual Data Report: Liver. Am J Transpl. 2024;24:S176-S265. https://doi.org/10.1016/j.ajt.2024.01.014.
20. Allen JW, Bhatia SN. Improving the next generation of bioartificial liver devices. Semin Cell Dev Biol. 2002;13:447–54. https://doi.org/10.1016/s1084952102001337.
21. Volarevic V, Nurkovic J, Arsenijevic N, Stojkovic M. Concise review: therapeutic potential of mesenchymal stem cells for the treatment of acute liver failure and cirrhosis. Stem Cells. 2014;32:2818–23. https://doi.org/10.1002/stem.1818.
22. Claria J, et al. Systemic inflammation in decompensated cirrhosis: characterization and role in acute-on-chronic liver failure. Hepatology. 2016;64:1249–64. https://doi.org/10.1002/hep.28740.
23. Bernsmeier C, van der Merwe S, Perianin A. Innate immune cells in cirrhosis. J Hepatol. 2020;73:186–201. https://doi.org/10.1016/j.jhep.2020.03.027.
24. Wu KKL, et al. The APPL1-Rab5 axis restricts NLRP3 inflammasome activation through early endosomal-dependent mitophagy in macrophages. Nat Commun. 2021;12:6637. https://doi.org/10.1038/s41467-021-26987-1.
25. Kim MJ, Yoon JH, Ryu JH. Mitophagy: a balance regulator of NLRP3 inflammasome activation. BMB Rep. 2016;49:529–35. https://doi.org/10.5483/bmbrep.
26. Chao X, Ding WX. Role and mechanisms of autophagy in alcohol-induced liver injury. Adv Pharmacol. 2019;85:109–31. https://doi.org/10.1016/bs.apha.2019.01.008.
27. Shan S, et al. Mitophagy protects against acetaminophen-induced acute liver injury in mice through inhibiting NLRP3 inflammasome activation. Biochem Pharmacol. 2019;169. https://doi.org/10.1016/j.bcp.2019.113643.
28. Jiang Z, et al. Sarmentosin promotes USP17 and regulates Nrf2-mediated mitophagy and cellular oxidative stress to alleviate APAP-induced acute liver failure. Phytomedicine. 2022;104:154337. https://doi.org/10.1016/j.phymed.2022.154337.
29. Zhao H, et al. Protective effects of fucoidan against ethanol-induced liver injury through maintaining mitochondrial function and mitophagy balance in rats. Food Funct. 2021;12:3842–54. https://doi.org/10.1039/d0fo03220d.
30. Allameh A, Niayesh-Mehr R, Aliarab A, Sebastiani G, Pantopoulos K. Oxidative stress in liver pathophysiology and disease. Antioxidants. 2023;12. https://doi.org/10.3390/antiox12091653.
31. Deng X, et al. Paeoniflorin protects hepatocytes from APAP-induced damage through launching autophagy via the mapk/mtor signaling pathway. Cell Mol Biol Lett. 2024;29. https://doi.org/10.1186/s11658-024-00631-4.
32. Long H, et al. Macrophages and fibrosis: how resident and infiltrating mononuclear phagocytes account for organ injury, regeneration or atrophy. Front Immunol. 2023;14. https://doi.org/10.3389/fimmu.2023.1194988.
33. Gkikas I, Palikaras K, Tavernarakis N. The role of mitophagy in innate immunity. Front Immunol. 2018;9. https://doi.org/10.3389/fimmu.2018.01283.
34. Zhang Y, et al. Mesenchymal stem cells alleviate bacteria-induced liver injury in mice by inducing regulatory dendritic cells. Hepatology. 2013;59:671–82. https://doi.org/10.1002/hep.26670.
35. Corcione A, et al. Human mesenchymal stem cells modulate B-cell functions. Blood. 2006;107:367–72. https://doi.org/10.1182/blood-2005-07-2657.
36. Milosavljevic N, et al. Mesenchymal stem cells attenuate acute liver injury by altering ratio between Interleukin 17 producing and regulatory natural killer T cells. Liver Transpl. 2017;23:1040–50. https://doi.org/10.1002/lt.24784.
37. Zhu X, He B, Zhou X, Ren J. Effects of transplanted bone-marrow-derived mesenchymal stem cells in animal models of acute hepatitis. Cell Tissue Res. 2012;351:477–86. https://doi.org/10.1007/s00441-012-1524-3.
38. Fang X, et al. A study about Immunomodulatory effect and efficacy and prognosis of human umbilical cord mesenchymal stem cells in patients with

chronic hepatitis B-induced decompensated liver cirrhosis. J Gastroenterol Hepatol. 2018;33:774–80. https://doi.org/10.1111/jgh.14081.
39. Zhu W, et al. Mesenchymal stem cells ameliorate hyperglycemia-induced endothelial injury through modulation of mitophagy. Cell Death Dis. 2018;9. https://doi.org/10.1038/s41419-018-0861-x.
40. Yang M, et al. Single-Cell transcriptome analysis of radiation pneumonitis mice. Antioxid (Basel). 2022;11. https://doi.org/10.3390/antiox11081457.
41. Cortal A, Martignetti L, Six E, Rausell A. Gene signature extraction and cell identity recognition at the single-cell level with Cell-ID. Nat Biotechnol. 2021;39:1095–102.
42. Andreatta M, Carmona SJ, UCell. Robust and scalable single-cell gene signature scoring. Comput Struct Biotechnol J. 2021;19:3796–8. https://doi.org/10.1016/j.csbj. 2021.06.043.

Publisher's note